AIP Journal of Applied Physics

Generation of uniform plasmas by crossed internal oscillating current sheets:Key concepts and experimental verification

E. L. Tsakadze, K. Ostrikov, Z. L. Tsakadze, and S. Xu

Citation: Journal of Applied Physics **97**, 013301 (2005); doi: 10.1063/1.1826214

View online: http://dx.doi.org/10.1063/1.1826214

View Table of Contents: http://scitation.aip.org/content/aip/journal/jap/97/1?ver=pdfcov

Published by the AIP Publishing

Generation of uniform plasmas by crossed internal oscillating current sheets: Key concepts and experimental verification

E. L. Tsakadze
Plasma Sources and Applications Center, NIE, Nanyang Technological University, 1 Nanyang Walk, 637616 Singapore and Optics and Plasma Research Department, Risø National Laboratory, P.O. Box 49, DK-4000 Roskilde, Denmark

K. Ostrikov[a)]
School of Physics, The University of Sydney, New South Wales 2006, Australia

Z. L. Tsakadze and S. Xu[b)]
Plasma Sources and Applications Center, NIE, Nanyang Technological University, 1 Nanyang Walk, 637616 Singapore

(Received 10 May 2004; accepted 11 October 2004; published online 9 December 2004)

The results of comprehensive experimental studies of the operation, stability, and plasma parameters of the low-frequency (0.46 MHz) inductively coupled plasmas sustained by the internal oscillating rf current are reported. The rf plasma is generated by using a custom-designed configuration of the internal rf coil that comprises two perpendicular sets of eight currents in each direction. Various diagnostic tools, such as magnetic probes, optical emission spectroscopy, and an rf-compensated Langmuir probe were used to investigate the electromagnetic, optical, and global properties of the argon plasma in wide ranges of the applied rf power and gas feedstock pressure. It is found that the uniformity of the electromagnetic field inside the plasma reactor is improved as compared to the conventional sources of inductively coupled plasmas with the external flat coil configuration. A reasonable agreement between the experimental data and computed electromagnetic field topography inside the chamber is reported. The Langmuir probe measurements reveal that the spatial profiles of the electron density, the effective electron temperature, plasma potential, and electron energy distribution/probability functions feature a high degree of the radial and axial uniformity and a weak azimuthal dependence, which is consistent with the earlier theoretical predictions. As the input rf power increases, the azimuthal dependence of the global plasma parameters vanishes. The obtained results demonstrate that by introducing the internal oscillated rf currents one can noticeably improve the uniformity of electromagnetic field topography, rf power deposition, and the plasma density in the reactor.
 [DOI: 10.1063/1.1826214]

I. INTRODUCTION

Plasma sources employing a variety of low-pressure (typically 1 mTorr–few Torr) gas discharges, including direct current (dc), wave-driven, microwave, radio-frequency (rf) discharges are extensively used by many industries for the processing of various dielectric, semiconductor, and conducting surfaces and bulk materials. Nowadays, the applications of the plasma discharges expand into the areas of synthesis of novel and advanced nanostructured and biocompatible materials with advanced functionalities.[1,2]

Inductively coupled plasmas (ICPs) is a subclass of rf gas discharges, which has recently attracted a great deal of interest as efficient sources of high-density ($>10^{11}-10^{12}$ cm^{-3}) low-temperature plasmas in large volumes and over large surface areas.[3–6] ICP discharges enable an independent control of the ion flux and ion-bombarding energy, high efficiency in terms of ionization and power utilization, and have several other attractive features, which make them promising sources of low-temperature plasmas for the semiconductor industry, synthesis of novel and advanced materials and fabrication of unique nanostructures.[7–17]

In the ICP reactors, the plasma is produced by rf electromagnetic fields generated by inductive coils of various configurations placed outside or inside the processing chamber. The rf power is coupled to the plasma inductively, via the excitation of rf currents in the chamber volume. The power that can be gainfully used for the plasma production critically depends on the configuration of the electromagnetic fields and rf currents excited in the chamber. Most of the existing ICP sources use 13.56 MHz rf generators to drive rf currents in the inductive coil.

However, some of the applications of the existing ICP devices suffer from nonuniformities of the main plasma parameters caused by nonuniform rf power deposition.[18] In particular, in the 13.56 MHz ICP devices employing flat spiral ("pancake") inductive coils, most commonly adopted in the semiconductor manufacturing, the above nonuniformities persist in the areas near the chamber axis. Secondly, generation and maintaining the uniformity of inductively coupled plasmas over large volumes has proved to be a troublesome

[a)]Also at Plasma Sources and Applications Center, NIE, Nanyang Technological University, 1 Nanyang Walk, 637616 Singapore.
[b)]Electronic mail: syxu@nie.edu.sg

problem.[19] This can result in substantial drawbacks in various applications of the ICP devices for technological processes that require a high level of uniformity over large volumes and surface areas. It is understood that this is intrinsic to most of external-coil configurations featuring noticeable depletion of the ion density along the axial direction.[20] Data on axial profiles of optical emission intensity (which is proportional to the number densities of species) of ionic and neutral argon species in the inductively coupled plasmas confirm that the ion density noticeably diminishes at distances less than a half of the chamber length.[20] Another shortcoming of the external-coil ICP configurations is a substantial rf power loss to the ambient, which also affects the power transfer efficiency.

Several attempts have been reported to solve the nonuniformity problem by modifying the rf power coupling, coil structures, or plasma confinement.[21–27] One of the possibilities to improve the uniformity of the power deposited into the plasma and plasma density is to generate internal rf currents with a spatially constant phase, also termed IOCs.[26]

This paper presents the results of the experimental investigation of the electromagnetic fields and plasma parameters in the inductively coupled plasma source with the internal oscillating current sheet. The operation and design of the plasma source are detailed. The experimental results confirm that the uniformity of the electromagnetic fields and power density, a troublesome problem in most conventional ICP sources, can indeed be improved by introducing a low-frequency internal current with a spatially constant phase. Moreover, the plasma can be generated with lower rf powers as compared to the plasma sources with external inductive coil configurations. Furthermore, the uniformity of the power density is improved and the rf power consumption is minimized.

The paper is organized as follows. In Sec. II the conceptual design of the plasma source with internal oscillating current is presented. Experimental details, such as experimental setup and various diagnostic tools, are described in Sec. III. Section IV addresses the issue of the rf power deposition and the electromagnetic field topography in the plasma source. The main plasma parameters, discharge operation modes, and the plasma source reproducibility are reported in Secs. V and VI, respectively. The key features of the new plasma source are discussed in Sec. VII. The paper concludes with a summary of the main results achieved and the outlook for the future research given in Sec. VIII.

II. CONCEPTUAL DESIGN OF THE PLASMA SOURCE AND ANTENNA CONFIGURATION

A schematic diagram of the plasma source with the IOC antenna configuration is shown in Fig. 1. To produce the unidirectional internal oscillating rf current inside the vacuum chamber, a new coil configuration has been designed. Contrary to conventional ICP sources with the external flat coil configuration, in the device reported here the internal rf antenna consists of the two orthogonal sets of copper litz wires placed inside a vacuum chamber. The wires are enclosed in fused silica tubes as shown in Fig. 2. The resulting rf current sheet thus oscillates in the r-φ plane of a

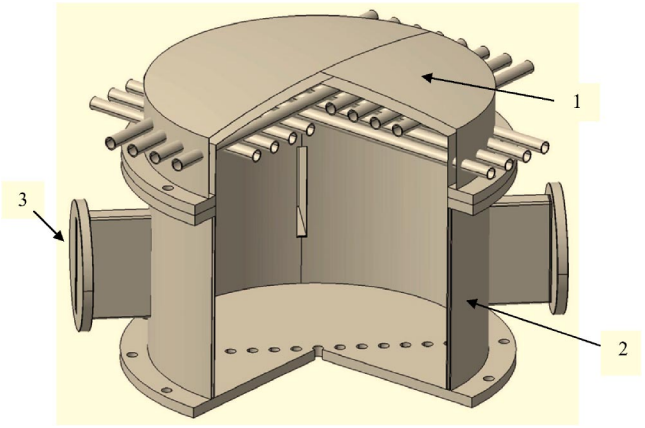

FIG. 1. 3D graphical representation with 1/4 isometric cut of the plasma source. Here, 1—top section of the vacuum chamber, 2—main section of the vacuum chamber, 3—diagnostic/observation porthole.

standard cylindrical coordinate system,[26] with the direction shifted $\sim 45^{\circ}$ with respect to either set of coils.

The total number of quartz tubes in each direction is 8 and all copper wires are connected in series. Note that the use of the two crossed unidirectional current sheets and the way how the orthogonally directed copper wires are reconnected reduces a power loss outside the plasma chamber. Due to the series connection and very low resistivity of the copper wires, the rf current is synphased in any part of the antenna. The inductive coil is made of 6 mm in diameter copper litz wire and is enclosed in quartz tubes with the inner and outer diameters of 10 and 12 mm, respectively. Figure 1 shows that one of the sets of eight quartz tubes is placed 3 cm above the top flange of the main section of the vacuum chamber, while the other set of 8 quartz tubes, which are perpendicular to the first one, is lifted up by 2 cm from the first set of wires. For convenience, the horizontal plane between the lower and upper sets of the coils was chosen as the origin for the axial axis ($z=0$), i.e., 4 cm above the top flange of the main section of the vacuum chamber. Figure 2 also illustrates the connections of the first two turns of the inductive coil and the resulting direction of the rf current oscillations.

It should be noted that, contrary to the conventional ICP case where the electric field has only the azimuthal component, the internal oscillating current generates an additional

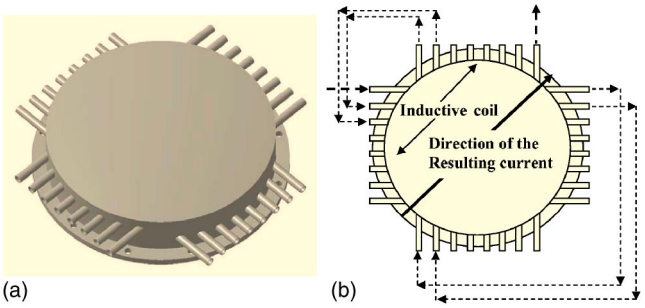

FIG. 2. 3D (a) and top (b) view of the rf antenna-carrying section of the plasma source. Reconnection of only two (in each direction) coil segments is shown (b). A solid arrow shows the direction of the resulting current oscillation in r-φ plane.

radial electric field and, therefore, the azimuthal magnetic field. One can thus expect that the presence of the additional electric field component will modify the power absorbed by the highly mobile plasma electrons.

III. EXPERIMENTAL DETAILS

A. Experimental setup

The rf antenna-carrying chamber top section (labeled 1 in Fig. 1) is mounted on the top flange of the main section of the vacuum chamber. The vacuum between the two different sections of the plasma reactor was sealed by a high-temperature resilient Viton O-ring.

The main section of the vacuum chamber (labeled 2 in Fig. 1) has a cylindrical shape with the diameter and height of 32 cm and 23 cm, respectively. Both sections of the plasma reactor are made of stainless steel and are double walled to allow cold water circulation to remove the excessive heat dissipation during the plasma discharges. Four rectangular ports (one of them is labeled 3 in Fig. 1) are symmetrically arranged around the circumference of the plasma chamber to facilitate visual monitoring of the discharge and enable the access of various plasma diagnostic tools, such as magnetic, single rf-compensated Langmuir, and optical emission probes. The diagnostic probes can be inserted radially at different vertical positions in the sideports, each of them has seven portholes separated by 2 cm in the axial direction. There are similar portholes in the aluminium bottom endplate of the plasma chamber. The endplate contains a set of 15 holes each separated by 2 cm, which allows the diagnostic probes to be inserted axially at various radial positions.

The plasma chamber is pumped through a small side port located at the lower portion of the vessel between two rectangular side ports. A KYKY (type 2XZ) turbomolecular pump (with a pumping speed of 450 l/s) backed by a two-stage rotary pump was used to evacuate the vessel. A typical routinely achievable base pressure can be as low as 5×10^{-5} Torr. A Pirani gauge (Edward model RM 10 with the measuring pressure range from 10^{3} to 10^{-3} Torr) and a Penning gauge (Edward model CP25K with the measuring pressure range from 10^{-3} to 10^{-8} Torr) were used to measure the base pressure. Both gauges were controlled by an Edward Pirani Penning readout (model 1005). Pure argon (99.99% purity) was used as a working gas. In order to control the flow rate of the working gas and the equilibrium pressure within the plasma chamber, MKS Flow Controllers 1100 series connected to MKS type 247C 4 Channel Readout were used. A MKS Baratron capacitance manometer (model 122AA), which was connected to a MKS type PDRC-2C power supply digital readout, was used to monitor the pressure inside the chamber. The working gas pressure p_0, which is typically in the range of 1–100 mTorr was controlled by a combination of a MKS flow controller and a manual gate valve equipped in the pumping line.

An Advanced Energy rf generator (model PDX 8000, 460 kHz) was used to drive the rf current in the antenna. The maximum output power of the generator is 8000 W into a 50 Ω, nonreactive load. However, the power supplied to the inductive coil in the experiment varied from 100 to 2500 W. The generator was connected to the coil via a specially designed π-type matching network. Two cooling units of type EYELA Cool Ace CA-1100 were used to supply cold water to both sections of the chamber, rf generator, and turbomolecular pump.

B. Diagnostic tools

To study the electromagnetic, global, and optical properties of the plasma source, a set of miniature magnetic probes, a single rf-compensated Langmuir probe, and optical emission spectroscopy were used.

1. Miniature magnetic probes

The electromagnetic properties of the internal oscillating current driven plasma source (IOC-PS) were studied by using two custom-designed miniature magnetic probes. The schematics and details of the magnetic probe design and operation can be found elsewhere.[28] Briefly, the key element of the probes is a miniature coil (with a different number of turns) wound around a Teflon frame mounted at the end of an aluminum tube with the internal diameter of 3 mm. Depending on the orientation of the probes, one of them can pick up the azimuthal or axial components of the magnetic field, while the other one can sense the radial magnetic field component. A continuous flow of compressed air was used to cool the probes. The air inflows through the aluminum tube and exits through the periphery space between the aluminum tube and the inner surface of the quartz feedthrough.

To minimize the effect of the rf interference on the magnetic probe signals, the aluminum tube was properly grounded. The spatial resolution of the probes was 0.6 cm, which enabled us to perform a detailed mapping of the rf magnetic field inside the plasma chamber.

2. Langmuir probe

Global plasma parameters were obtained from the time-resolved measurements by a single rf-compensated cylindrical Langmuir probe. The probe was powered by ac (50 Hz) voltage in the range from −40 to +40 V through a variable transformer. To isolate the electric connection between the probe and main power supply an additional isolation transformer (with 1:1 ratio) was used. The probe voltage across the plasma load resistance was measured by a Tektronix voltage probe and monitored on a digital storage oscilloscope (Tektronix model 380) via a 1.0 MHz low-pass filter. The probe current was obtained by measuring the voltage drop across a 0.26 Ω resistor and monitored on the same oscilloscope via a 0.2 MHz low-pass filter. All the obtained signals were transmitted to a PC via the GPIB port of the oscilloscope. A PC-based data acquisition system was used to record and process the data, and obtain the electron density, effective electron temperature, plasma potential, and electron energy distribution/probability functions (EEDF/EEPF). The main plasma parameters were determined by using the second derivative of the Langmuir probe current-voltage characteristics (Druyvestein routine).[4,29] We note that the reproducibility of the data collected was excellent. All the diagnostic tools and data acquisition system were electro-

statically shielded to minimize any rf interference from the generator and antenna rf fields. Since the plasma chamber provides a good reference ground for the single rf-compensated Langmuir probe measurements in the electron collection voltage range, the plasma potential and effective electron temperature can be accurately obtained from the measured *I-V* probe characteristics.[29]

3. Optical emission spectroscopy

Optical characteristics of the plasma generated in the IOC-PS were investigated at different input rf powers and gas feedstock pressures. The optical emission spectra from argon gas in the wavelength range of 300–900 nm were studied. The variation of the optical emission intensity of different atomic/ion lines in the argon plasma was dynamically monitored while the coil current was varied. The optical emission of different spectral lines of the excited/ionized species produced by the plasma discharge were collected by a collimated optical probe inserted radially or axially into the plasma chamber. An optical fiber was used to transmit the collected signal to the entrance slit of a monochromator (Acton Research SpectraPro-750i model, 0.750 m focal length triple grating imaging monochromator/spectrograph). The emission was amplified by a photomultiplier and then dispersed and analyzed by the monochromator (with a spectral resolution of 0.023 nm) in the preset wavelength range. The amplitude of the output signal from the photomultiplier could be changed by adjusting the voltage output from a high-voltage generator. In order to monitor the output signal on the computer in real time, the signal was continuously digitized by an A/D convertor buit-in in the scan controller. The scanning and data acquisition process were controlled by the data acquisition and analysis software Spectrasense™ (Acton Research Corporation). Using the data acqusition system, we were able to record broad spectral bands or selectively monitor certain spectral lines.

IV. RF POWER DEPOSITION

By using the rf coil configuration of our interest here, one can inductively generate all three components H_r, H_φ, and H_z of the magnetic field, and two components E_r and E_φ of the electric field. The plasma current, with the radial J_r and azimuthal J_φ components, is generated by the internal unidirectional current sheet. The rf magnetic field in the plasma is generated by the antenna currents and the rf plasma currents induced in the plasma bulk. The contribution of the plasma currents is the strongest in the high-density plasma case. On the other hand, low-density plasmas are highly transparent to the rf field and the induced plasma currents are usually quite weak.

The distribution of the electromagnetic field was studied by the miniature magnetic probes. The details on the measurements of the magnetic field topography in the IOC-PS can be found elsewhere.[31,32] Radial scans of the magnetic field components were made at the following axial and azimuthal positions: (1) $z=8$, 14 cm and $\varphi=90°$ (perpendicular to the internal oscillating rf current), (2) $z=8$ cm and $\varphi=0°$ (along the IOC). Measurements by one of the probes allow one to obtain the radial dependence of the radial H_r and axial H_z components of the magnetic field, while the second magnetic probe yields the azimuthal H_φ component of the magnetic field as a function of the radial position. The magnetic field topography inside the plasma chamber was investigated for the evacuated, rarefied, and dense plasma cases. It was found that the difference between magnetic field distributions in the first two cases was minor. For this reason, in this section we will focus on the results of the field topography in the dense plasma case.

Contrary to the evacuated and rarefied plasma cases, where the electron density is not high enough to inhibit a deep penetration of the electromagnetic field into the plasma, in the dense plasma case the screening effect becomes stronger. It affects the field distribution inside the chamber and results in the localization of the field near the source of excitation. Along with the above screening effect, various nonlinear effects, such as the generation of high harmonic components of the magnetic field, ponderomotive forces and other effects, become more pronounced. These effects also modify the field distribution in the chamber. Figs. 3 and 4 show the radial profiles of the radial, axial, and azimuthal components of the magnetic field inside the vessel fully filled by a dense ($\sim 6\times 10^{11}$ cm^{-3}) argon plasma. The values of the gas pressure and power deposition into the plasma are 30 mTorr and $\sim$0.6 kW, respectively.

For comparison, the computed distributions of the corresponding components of the magnetic fields are also depicted in the figures (solid line).[26] The discrepancy between the numerical and experimental results can be attributed to strong nonlinear plasma effects at low rf frequencies and gas pressures, which were not accounted for in the numerical model.[26]

The axial dependence of the magnetic field components was also studied. The axial scans of the magnetic components were performed at the following radial and azimuthal positions: (a) $r=0$, 8 cm and $\varphi=90°$ (perpendicular to the IOC), (b) $r=0$ cm and $\varphi=0°$ (parallel to the IOC) and the obtained results are depicted in Fig. 5. Figure 5 shows that the axial profiles of the radial and azimuthal components of the magnetic field change dramatically by switching the discharge from the electrostatic *E* to the electromagnetic *H* mode. Indeed, in the *E*-mode discharge only a smooth decay of all the magnetic field components with the axial distance *z* can be observed. On the other hand, in the dense electromagnetic discharge mode, we have observed a rise of the H_r and H_φ with *z* at the axial distances $z>14-15$ cm.[31,32] We emphasize that the observed rise of the amplitudes of magnetic fields with the axial distance is not common for conventional sources of inductively coupled plasmas and can be attributed to the excitation of the plasma eigenmodes propagating along the axial direction. On the other hand, the axial profile of the H_z [Fig. 5(c)] becomes smoother and more uniform compared to the corresponding profile in the *E*-mode discharge.[31,32]

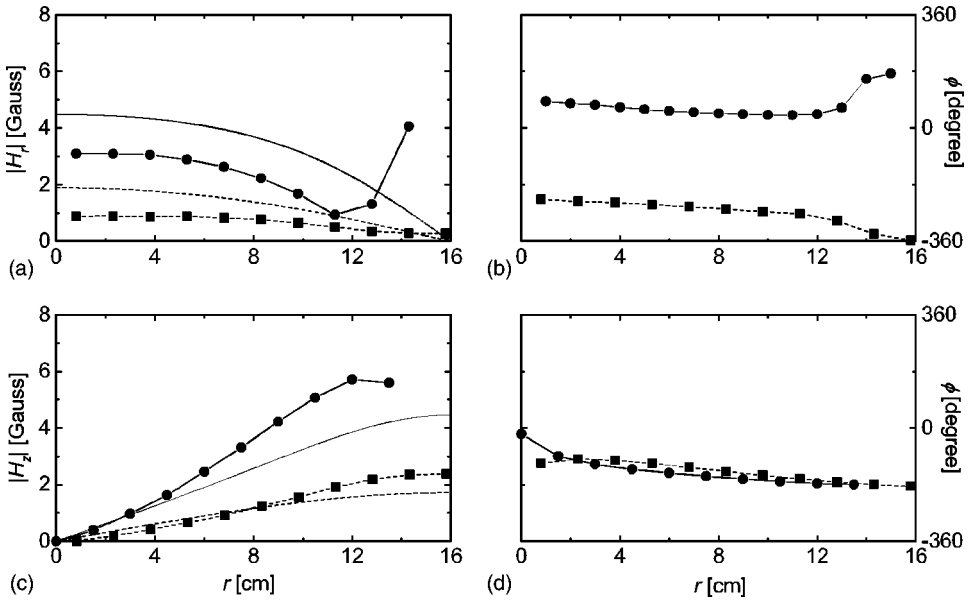

FIG. 3. Experimentally measured (circle, square) and computed (solid and dash lines) radial dependences of the absolute values (a), (c) and phase (b), (d) of the induced radial (a), (b) and axial (c), (d) components of the magnetic field in the chamber filled by a dense plasma. Coil current and argon gas pressure are 24 A and 51 mTorr, respectively. The measurements have been performed at axial distance $z=8$ cm (circle, solid line) and 14 cm (square, dash line) and azimuthal angle $\varphi=90°$.

V. PLASMA PARAMETERS IN THE IOC PLASMA SOURCE

The experimental data on the global plasma parameters were obtained from the time resolved measurements by a single rf-compensated cylindrical Langmuir probe. The plasma density n_e, effective electron temperature T_{eff}, and plasma potential V_p were determined by using the Druyvestein routine.[4] In particular, n_e and T_{eff} can be expressed as

$$n_e = \int g_e(V)dV, \quad T_{\text{eff}} = \frac{2}{3n_e}\int Vg_e(V)dV,$$

energy distribution function $g_e(V)$ can be obtained through the second derivative of the probe current over the voltage d^2I_e/dV^2 as

$$g_e(V) = \frac{2m_e}{e^2A}\left(\frac{2eV}{m_e}\right)^{1/2}\frac{d^2I_e}{dV^2},$$

where e, m_e, and A are the elementary charge, electron mass and the probe surface area.

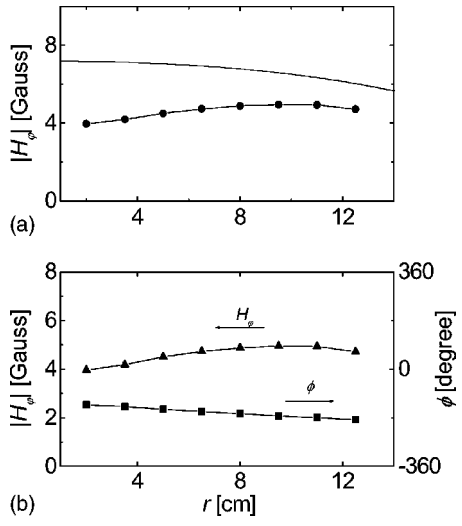

FIG. 4. Same as in Fig. 3, for the azimuthal magnetic field component.

The plasma potential V_p can be found as the maximum of the first derivative of the dependence $I(V)$ or as the zero crossing point of the second derivative of the probe current.[4]

Figure 6 shows the radial (a) and axial (b) distributions of the electron density, effective electron temperature and plasma potential in the electromagnetic H mode of a pure argon discharge and for the azimuthal angle $\varphi=0°$, which is the direction of the resulting oscillating rf current. One can see that the value of n_e remains almost the same for radial positions r from 0.5 to 7.5 cm [Fig. 6(a)] and then starts to decrease. The typical values of the plasma density for the

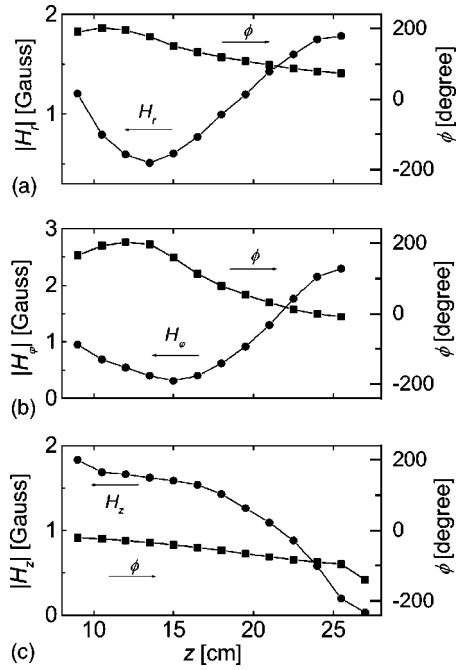

FIG. 5. Axial profiles of the radial (a), azimuthal (b), and axial (c) components of the magnetic field in the plasma chamber fully filled by a dense argon plasma ($n_e \sim 6\times10^{11}$ cm^{-3}). Coil current and argon pressure is 24 A and 30 mTorr, respectively. Here, circles and squares correspond to absolute values of the measured components of the magnetic field and phase difference between them and rf coil current, respectively.

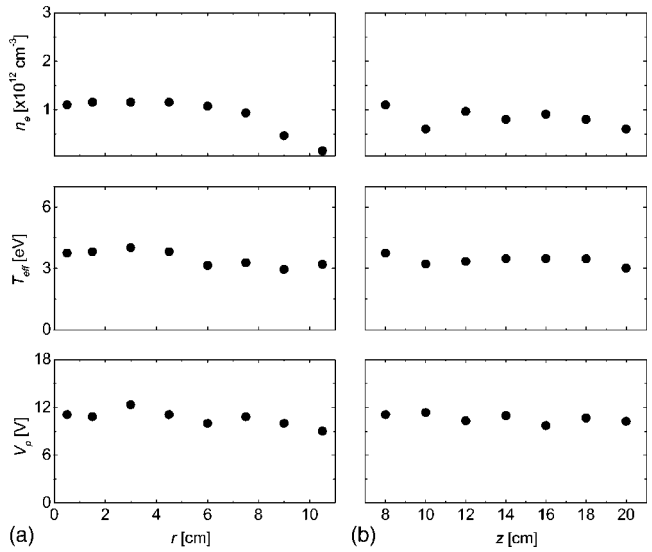

FIG. 6. Radial (a) and axial (b) profiles of the electron density n_e, the effective electron temperature T_{eff}, and plasma potential V_p, for the *H*-mode argon discharge with rf power input $P_p \sim 1.6$ kW and gas pressure, $p_0 = 51$ mTorr, respectively. All profiles are plotted for axial (a) and radial (b) positions $z = 8$ cm and $r = 0.5$ cm, and azimuthal angle $\varphi = 0°$.

discharge are 1.1×10^{12} and 0.7×10^{12} cm^{-3} for the gas feedstock pressures 51 and 30 mTorr, respectively. Meanwhile, the plasma potential and effective electron temperature are almost constant along the chamber radius.

The measurements of the axial profiles of the global plasma parameters [Fig. 6(b)] were performed at seven different axial positions through the available portholes in the diagnostic side port. It was found that n_e, T_{eff}, and V_p remain fairly uniform along the *z* axis from 8 to 20 cm. Thus, one can clearly see that the introduction of the unidirectional internal rf current into the plasma indeed improves the spatial uniformity of the plasma generated.

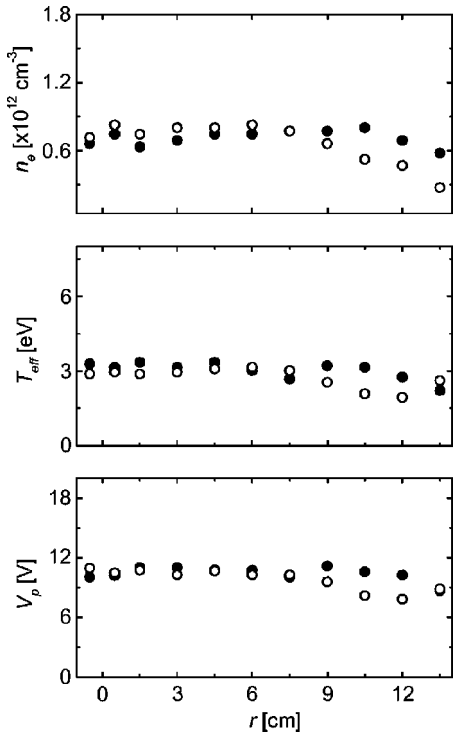

FIG. 7. Radial profiles of the electron density, the effective electron temperature and plasma potential for the *H*-mode argon discharge with rf power input $P_p = 0.62$ kW and gas filling pressure $p_0 = 51$ mTorr, respectively. All profiles are plotted for axial position $z = 12$ cm and azimuthal angle $\varphi = 0°$ (solid circles) and 90° (hollow circles).

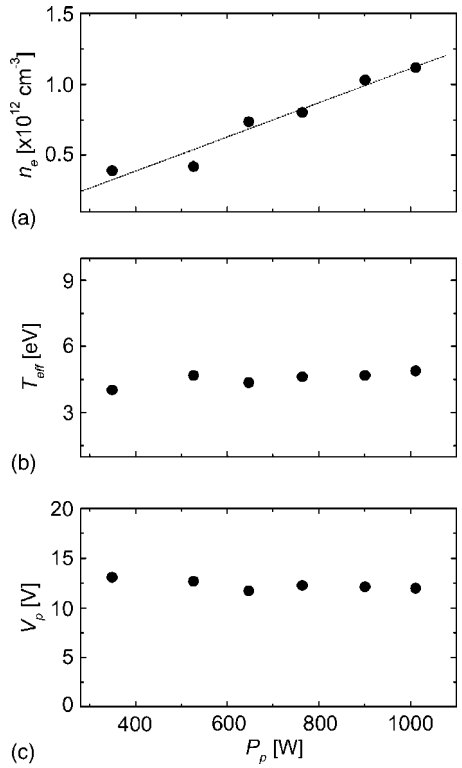

FIG. 8. The dependence of the electron density, effective electron temperature, and plasma potential on the input rf power for the *H*-mode argon discharge and for gas filling pressure $p_0 = 51$ mTorr. The Langmuir probe was located at $r = 0.5$ cm and $z = 12$ cm.

Furthermore, the plasma source of our interest here offers a great deal of control of the plasma parameters along the azimuthal direction.[26] In order to investigate the azimuthal dependence of the plasma density, plasma potential, and effective electron temperature, the Langmuir probe measurements were carried out for the azimuthal angles $\varphi = 0$ and 90°. We have observed that the rf power density features a weak azimuthal dependence at low rf powers as shown in Fig. 7. Note that this gives the possibility to control the rf power deposition in the processes that require the azimuthal profiling of the film thickness or etch rate. It was further observed that the azimuthal dependence of the global plasma parameters disappears with an increase of the rf power.

The dependence of the global plasma parameters on the input rf power at different gas pressures was also studied. For instance, the results for $p_0 = 51$ mTorr are shown in Fig. 8. In this case the tip of the Langmuir probe was located at the radial and axial positions 0.5 and 12 cm, respectively. In particular, the electron number density was found linearly proportional to the net rf power input in the established electromagnetic mode within the input power range of 0.5–1.0 kW. This is consistent with earlier numerical models of the of the plasma source with the internal oscillating currents,[26] and extensive experimental and theoretical studies of conventional inductively coupled plasma sources with flat

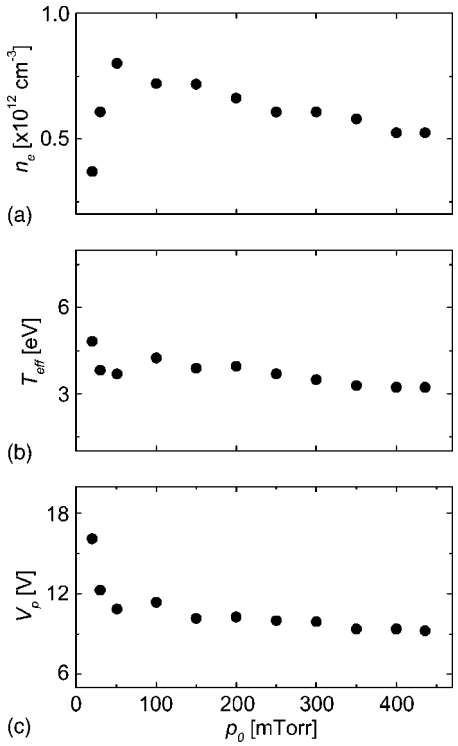

FIG. 9. The effect of the gas pressure on the electron density, effective electron temperature and plasma potential for *H*-mode argon discharge and for rf input power $P_p \sim 0.68$ kW. The Langmuir probe position is the same as in Fig. 8.

external coil configurations (see, e.g., Xu *et al.*[33] and references therein). Meanwhile, in the same rf power range the effective electron temperature appears to be a slowly increasing function of the rf power, whereas the plasma potential remains almost invariable with power.

The effect of the gas feedstock pressure on n_e, T_{eff}, and V_p was also studied. Figure 9 shows the global plasma parameters as a function of p_0 for the *H*-mode argon discharge at a constant rf power input $P_p = 0.68$ kW. Note that the Langmuir probe position during the measurements was the same as in Fig. 8. As one can see from Fig. 8, in the pressure range below 51 mTorr, the electron density increases with pressure from 3.7×10^{11} cm^{-3} at 20 mTorr to 8.0×10^{11} cm^{-3} at 51 mTorr. In the pressure range exceeding 51 mTorr, the electron density starts to decline with the pressure and its value decreases from 8.0×10^{11} cm^{-3} at 51 mTorr to 5.2×10^{11} cm^{-3} at ~440 mTorr. Note that at rf input power 0.68 kW the flex point corresponds to $p_0 = 51$ mTorr. It should also be noted that the rate of change of the plasma density with p_0 in the range above 51 mTorr is much slower than in the lower pressure range ($p_0 < 51$ mTorr). As the pressure increases from 20 to 51 mTorr, the plasma potential drops rapidly from 16.1 to 10.8 V. However, V_p decreases slowly with p_0 in the range above 51 mTorr. The electron temperature follows a similar tendency. Initially, T_{eff} drops from 4.8 eV at $p_0 = 20$ mTorr to 3.7 eV at $p_0 = 51$ mTorr. Thereafter, the electron temperature continues to decrease and also experiences small fluctuations.

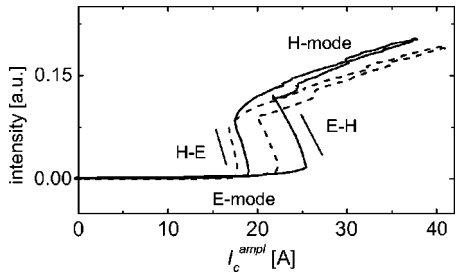

FIG. 10. Variation of the optical emission intensity of neutral Ar line (840.82 nm) during the $E \rightarrow H$ mode transition and inverse $H \rightarrow E$ mode transition for different gas pressures. Solid and dash lines correspond to gas pressure 40 and 50 mTorr, respectively.

VI. DISCHARGE OPERATION MODES AND REPRODUCIBILITY

It was observed that, similar to many conventional ICP sources, the IOC-PS can generate and sustain the plasma in two distinctive discharge regimes, namely, the electrostatic *E* and electromagnetic *H* modes. In particular, Fig. 10 illustrates a cyclic variation of the optical emission intensity (OEI) of the 840.82 nm neutral Ar line with the rf coil current for different gas pressures. One can easily notice that the $E \rightarrow H$ transition is accompanied by an instantaneous increase of the OEI. The OEI further increases with the coil current in the established *H*-mode regime. When the coil current is reduced, the OEI decreases almost linearly. For certain values of the rf coil current below the threshold of the $E \rightarrow H$ transition, the discharge still remains in the bright electromagnetic mode. However, when the point of the $H \rightarrow E$ transition is reached, the optical emission intensity sharply drops to the level corresponding to the electrostatic mode. In the electrostatic regime, the OEI does not change much and remains low compared to the *H*-mode discharges. Generally speaking, the feature of forming hysteresis loops is peculiar to many inductively coupled plasma sources.[33,34] It was further observed that the spectral lines in both discharge modes in the IOC-PS have higher intensities (Fig. 11) as compared to conventional ICP sources with external flat spiral coils. This is particularly true for the electrostatic discharge mode, which appears much brighter than the E-mode discharges in conventional ICPs under the same conditions.

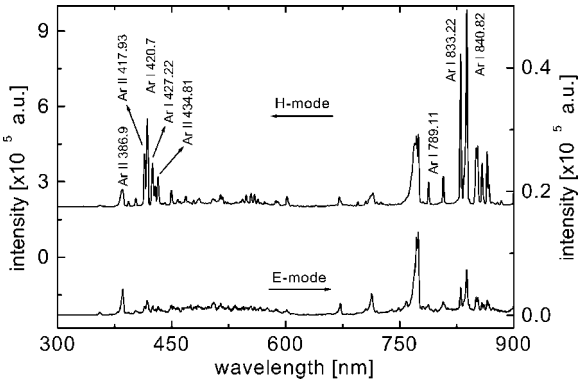

FIG. 11. Optical emission spectra from a 22 mTorr pure argon discharge in the *H*-mode operating regime sustained with 0.88 kW input power (upper curve) and in the *E*-mode operating regime sustained with 0.38 kW input power, respectively. Optical probe was located at $z = 10$ cm.

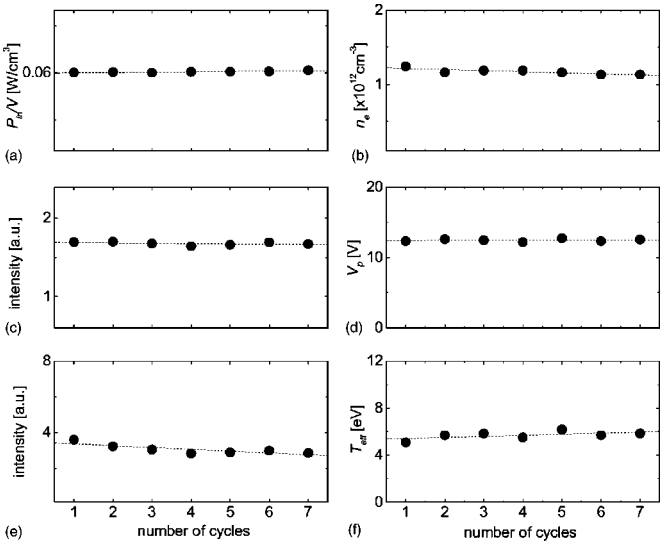

FIG. 12. Reproducibility of the rf power density (a), electron number density (b), optical emission intensity of neutral argon atoms (840.82 nm) (c), plasma potential (d), optical emission intensity of an argon ion (386.9 nm) (e), and effective electron temperature (f). The coil current and operational pressure are 31 A and 51 mTorr, respectively.

One of the essential characteristics of any plasma processing device is the reproducibility of its characteristics. Indeed, in most material processing applications, the plasma source must feature a sound reproducibility of the electrical, optical, and global plasma parameters. In order to examine the reproducibility of the main parameters of the plasma source of our interest here the following set of experiments was carried out. The processing chamber was first evacuated to $\sim 2\times 10^{-4}$ Torr. The working gas was then introduced into the plasma chamber and pressure of 51 mTorr was maintained invariable during the experiment. The rf generator was turned on and the coil current was increased up to the fixed value $I_c \sim 31$ A, when a very bright *H*-mode plasma was generated. Using a single rf-compensated Langmuir probe, OES, and voltage and current probes, the global, optical, and electrical properties of the plasma were measured. Thereafter, the rf generator was turned off and the gas feedstock inlet was discontinued. A vacuum pumping system was also switched off and pure argon was introduced in the chamber to let the pressure inside the vessel equalize with the atmospheric one. The above routine was repeated seven times to exam the reproducibility of the plasma parameters in the IOC-PS. A typical duration of each cycle was ≈ 1 h.

The main plasma parameters such as the electron density, effective electron temperature, and plasma potential were measured using a single rf-compensated Langmuir probe inserted radially and along the direction of rf current oscillation (marked by the arrow in Fig. 2). The tip of the Langmuir probe was positioned at $r=0$ and $z=12$ cm. At the same time, the intensities of the neutral (840.82 nm) and ionized (386.9 nm) argon lines were monitored by the optical probe inserted axially through the central hole in the bottom plate $(r=0)$.

Figure 12 illustrates the reproducibility of the rf power density in the reactor chamber, optical emission intensities of selected neutral and ionized argon lines, and main plasma parameters from one experiment to another. As can be seen from Fig. 12, the plasma density, electron temperature, and plasma potential remained the same. For the rf coil current $I_c \sim 31$ A, $P_p \sim 1.7$ kW, and $p_0 \sim 51$ mTorr, the values of n_e, T_{eff}, and V_p were $\sim 1.1\times 10^{12}$ cm^{-3}, 5.5 eV, and 12.2 eV, respectively. Therefore, Fig. 12 demonstrates the excellent reproducibility of the main plasma parameters in the plasma source of our interest here.

VII. DISCUSSION

We now discuss the effect of the internal oscillating rf current on the field distribution, power deposition, and plasma parameters and pinpoint the major advantages of the IOC-PS over conventional sources of inductively coupled plasmas with with external flat spiral coils.

In this work the plasma is generated by means of internal orthogonal unidirectional oscillating rf current sheets inside a vacuum chamber. The current sheets produce a time-varying rf electric field, which is azimuthally shifted on 45° with respect to the directions of both sets of current-carrying wires. Physically, the introduction of an oscillating rf current inside the vacuum chamber significantly affects the electromagnetic field distribution, rf power deposition and modifies the parameters of the plasma produced. In this particular internal rf antenna arrangement, the generated electric field oscillates in the $r-\varphi$ plane. Thus, the generated electromagnetic field has all three components of the magnetic field and two components (radial and azimuthal) of the electric field. On the other hand, the inductively driven rf current inside the chamber should also oscillate in the r-φ plane. However, since the current must form a closed loop, it is most likely that the return current path will be in the r-z (commonly termed "poloidal" in nuclear fusion devices) plane. This can be the reason of a deep penetration of the current into the plasma. Indeed, the experimental study of the field topography in the dense plasma case (Fig. 3) confirms this.

A comparison of the experimentally measured and computed radial and axial profiles of the electromagnetic fields shows a remarkable agreement in the low-density plasma *E*-mode discharge.[26,31] In particular, when the plasma density is $\sim 4\times 10^{9}$ cm^{-3} or less, the electromagnetic field profiles in the plasma are almost the same as in the fully evacuated vacuum chamber.[31] Hence, the low-density plasma is transparent to the electromagnetic field. A comparison of the computed and experimentally measured radial profiles of the electromagnetic field components in the *H*-mode discharge (Figs. 3 and 4) also shows a reasonable agreement. However, there is a noticeable discrepancy between the experimental and numerical axial profiles in Fig. 5. This discrepancy can be attributed to a number of non-linear effects in the electromagnetic field penetration into the dense plasma, which were not accounted for in the numerical studies.[26] The above nonlinear effects, including but not limited to the generation of strong second harmonic currents in the plasma, nonlinear Lorentz and ponderomotive forces, can be strong in the low-frequency, low-pressure operation regime of the IOC-PS, and noticeably affect the electromagnetic field distribution in the plasma chamber.

Another serious concern in the existing ICP devices is the axial uniformity of the main plasma parameters required for large-volume plasma processing applications. In particular, this problem can be overcome by enhancing the rf magnetic field penetration due to essentially nonlinear effects.[9,35,36] Physically, in the planar external-coil ICP geometry the nonlinear poloidal currents j_{er} and j_{ez} generate a strongly nonlinear azimuthal magnetic field H_φ, which does not have a fundamental-frequency Fourier component.[36] This effect has recently been confirmed experimentally.[33] Above all, finite H_φ can result in the enhanced penetration of the rf field due to *secondary* nonlinear effects (the meaning of the terms "primary" and "secondary" nonlinear effects is explained elsewhere[36]), which become even stronger at lower operation frequencies.[37] The indisputable advantage of the rf current configuration of our interest here is that the poloidal rf current and hence, the azimuthal magnetic field are driven in a linear fashion at the fundamental frequency and the enhanced rf field penetration can be achieved due to *primary* nonlinear effects. Furthermore, the internal oscillating current eliminates the non-uniformity of the rf power density in the vicinity of the chamber axis, which is inherent to many inductively coupled plasma sources with external flat spiral rf coils.[20,38] Driving the oscillating rf current inside the chamber one can achieve a substantially better uniformity of the rf power transferred to the plasma electrons as compared with the inductively coupled plasma devices with an external flat coil (see, e.g., Figs. 8 and 9 of Tsakadze *et al.*[26]).

On the other hand, one can expect that the azimuthal variation of the rf power deposited to the plasma can result in spatial nonuniformities of the ionization source, and hence, the electron temperature. In particular, this can lead to heat flows $Q=(5n_eT_e/2m_e\nu_e)\nabla T_e$ that can substantially modify the power balance in the discharge and be the reason for frequently observed deviations of the electron/ion number density profiles from the one obtained by using the conventional diffusion theory of low-temperature plasma glow discharges. Indeed, the experimental study of the global parameters of the plasma generated in the IOC-PS shows that the plasma density is a function of the azimuthal angle at lower values of the input power. However, this dependence disappears with an increase of the power absorbed by the plasma.

We recall that the electromagnetic field generated inside the chamber of the IOC-PS features all three components $H_r(r,\varphi,z)$, $H_\varphi(r,\varphi,z)$, and $H_z(r,\varphi,z)$ of the magnetic field and two electric field components $E_r(r,\varphi,z)$ and $E_\varphi(r,\varphi,z)$. The comparison of the rf power density in the conventional ICP source and the IOC-PS (under the same conditions) reveals that the power absorbed by the plasma electrons in the conventional ICP source is strongly nonuniform near the chamber axis [see, e.g., Fig. 7(b) of Tsakadze *et al.*[23] or Fig. 12 of Khater and Overzet[24]], whereas the rf power density profiles in the IOC-PS feature excellent radial uniformity.

The results of our experimental studies suggest that a uniform deposition of the rf power into the plasma results in the outstanding spatial uniformity of the main plasma parameters. The measurements conducted by a single rf-compensated Langmuir probe demonstrate a high degree of radial and azimuthal uniformity of the electron density, effective electron temperature, and plasma potential over the surface and volume areas of the reactor chamber (Figs. 6 and 7). Meanwhile, the IOC-PS is capable to generate and sustain high-density plasmas ($\sim 10^{12}$ cm^{-3}) with relatively lower values of the input rf power.

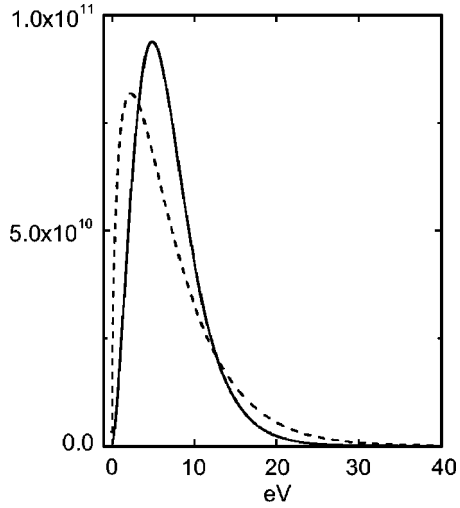

FIG. 13. Electron energy distribution function for power input $P_p \sim 0.62$ kW, gas pressure $p_0 \sim 51$ mTorr, axial and radial positions 12 and 10.5 cm, respectively, and $\varphi = 0°$. Solid and dash lines present the experimentally measured and the corresponding Maxwellian EEDFs (plotted for the same experimental conditions), respectively.

In this work, the values of the plasma density, effective electron temperature, and plasma potential were derived from the measured *I-V* characteristic of a single rf-compensated Langmuir probe by using the Druyvesteyn routine.[29] It is interesting to note that using the assumption of Maxwellian electrons and a simple expression for the ion probe current in the ion collection range of the *I-V* curve, the value of the electron number density can be overestimated in up to two times. This is yet another indication that the plasma of our interest here features non-Maxwellian electrons. This is consistent with the results of our EEDF measurements indicating that that the actual electron energy distribution function in the discharge is more likely Druyvestein-like rather than Maxwellian-like (Fig. 13).

Similarly to other inductively coupled plasma sources, the IOC-PS features two distinctive operation modes. The transition between the electrostatic *E* and electromagnetic *H* modes reveals pronounced hysteresis phenomena, which become stronger at lower operating pressures. We note that the intensity of nonlinear and nonlocal kinetic effects in the low-pressure domain is usually higher.[39] It was also observed that the intensities of different spectral lines of argon discharge were higher (in both *E* and *H* discharge modes) compared to conventional ICP sources with external flat spiral coil configurations. Presumably, this can be attributed to more efficient rf power transfer from the antenna to the plasma in the IOC-PS.

It is also interesting to note that the IOC plasma source can be easily converted into a conventional ICP source by replacing the chamber top (labeled 1 in Fig. 1) by a reasonably thick fused silica window and installing a flat spiral antenna coil above it. In conventional ICP sources with the

external flat spiral antenna the coil usually sits horizontally just above (usually ~1 cm) the fused silica window.[28] The minimum thickness of the window depends on the size of the reactor and the lowest achievable base pressures in the vacuum chamber. For example, for the chamber of our interest here and base pressures of the order of 10^{-5} Torr, the fused silica window should be at least 1.5 cm thick to withstand the atmospheric pressure load. A typical cost of such a window is a few thousand dollars. On the other hand, the plasma source of our interest here does not need any dielectric windows, which makes it a cost-efficient alternative to many conventional plasma sources.

Finally, from the application point of view, one can expect the outstanding uniformity, efficiency, flexibility, and reproducibility of the plasma reactor in large area semiconductor processing, LCD panel manufacturing, surface hardening and modification, biotechnology and nanotechnology, where high degree of the plasma uniformity not only over large cross sections, but also over large volumes is essential.

VIII. CONCLUSION

A new plasma source with the IOC antenna configuration was developed and tested. The electromagnetic, optical, and global parameters of the plasma generated were experimentally investigated. It was confirmed that the IOC-PS is capable to generate high-density low-temperature plasma with a high degree of spatial uniformity. It was also found that by introducing the internal antenna configuration one can control the rf power deposition in the azimuthal direction. This effect is more pronounced at lower rf input powers, which is consistent the earlier numerical models of the IOC-PS. Moreover, by introducing the internal inductive coil, one makes the quartz window (which is an expensive and essential part of the conventional ICP sources with the external flat spiral coil antenna configurations), redundant and improves the confinement of the magnetic flux inside the chamber. Finally, distinctive features of the ICP source with the internal oscillating rf current makes it promising for various plasma processing applications.

ACKNOWLEDGMENTS

This work was supported by the Agency for Science, Technology, and Research of Singapore (Project No. 01210100247) and the Australian Research Council.

[1]G. S. Oehrlein, *Plasma Processing of Electronic Materials* (Springer, Berlin, 2003).
[2]S. V. Vladimirov and K. Ostrikov, Phys. Rep. **393**, 175 (2004).
[3]O. Auciello, A. Gras-Marti, J. A. Valles-Abarca, and D. L. Flamm, *Plasma-Surface Interactions and Processing of Materials* (Kluwer, Boston, 1990).
[4]M. A. Lieberman and A. J. Lichtenberg, *Principles of Plasma Discharges and Materials Processing* (Wiley, New York, 1994).
[5]J. Hopwood, Plasma Sources Sci. Technol. **1**, 109 (1992).
[6]J. H. Keller, Plasma Phys. Controlled Fusion **39**, A437 (1997).
[7]C. Y. Chang and S. M. Sze, *ULSI Technology* (McGraw-Hill, New York, 1996).
[8]M. C. Roco, S. Williams, and P. Alivisatos, *Nanotechcnology research Directions: Vision for Nanotechnology, Research, and Development in the Next Decade* (Kluwer Academic, Amsterdam, 1999).
[9]M. Tuszewski, Phys. Plasmas **5**, 1198 (1998).
[10]M. A. Lieberman and V. A. Godyak, IEEE Trans. Plasma Sci. **26**, 955 (1998).
[11]L. Delzeit, I. McAninch, B. A. Cruden, D. Hash, B. Chen, J. Han, and M. Meyyappan, J. Appl. Phys. **91**, 9 (2002).
[12]Z. Shen, T. Kim, U. Kortshagen, P. H. McMurry, and S. A. Campbell, J. Appl. Phys. **94**, 4 (2003).
[13]A. Bapat, C. R. Perrey, S. A. Campbell, C. B. Carter, and U. Kortshagen, J. Appl. Phys. **94**, 1969 (2003).
[14]L. Y. Chen and F. C. N. Hong, Appl. Phys. Lett. **82**, 3526 (2003).
[15]J. B. O. Caughman, L. R. Baylor, M. A. Cuillorn, V. I. Merkulov, D. H. Lowndes, and L. F. Allard, Appl. Phys. Lett. **83**, 1207 (2003).
[16]T. N. Oder, K. H. Kim, J. Y. Lin, and H. X. Jiang, Appl. Phys. Lett. **84**, 466 (2004).
[17]F. Pommereau *et al.*, J. Appl. Phys. **95**, 2242 (2004).
[18]J. A. Stittsworth and A. E. Wendt, Plasma Sources Sci. Technol. **5**, 429 (1996).
[19]M. Tuszewski, IEEE Trans. Plasma Sci. **27**, 68 (1999).
[20]K. N. Ostrikov, S. Xu, and A. B. M. Shafiul Azam, J. Vac. Sci. Technol. A **20**, 251 (2002).
[21]Y. Wu and M. A. Lieberman, Appl. Phys. Lett. **72**, 777 (1998).
[22]S. S. Kim, H. Y. Chang, and C. S. Chang, Appl. Phys. Lett. **77**, 492 (2000).
[23]E. L. Tsakadze, K. N. Ostrikov, S. Xu, I. R. Jones, R. Storer, M. Y. Yu, and S. Lee, Phys. Rev. E **63**, 046402 (2001).
[24]M. H. Khater and L. J. Overzet, Plasma Sources Sci. Technol. **9**, 545 (2000).
[25]Y. Setsuhara, S. Miyake, Y. Sakawa, and T. Shoji, Jpn. J. Appl. Phys., Part 1 **38**, 4263 (1999).
[26]E. L. Tsakadze, K. N. Ostrikov, S. Xu, R. Storer, and H. Sugai, J. Appl. Phys. **91**, 1804 (2002).
[27]I. M. El-Fayoumi, I. R. Jones, and M. M. Turner, J. Phys. D **31**, 3082 (1998).
[28]K. Ostrikov, E. Tsakadze, S. Xu, S. V. Vladimirov, and R. Storer, Phys. Plasmas **10**, 1146 (2003).
[29]V. A. Godyak, R. B. Piejak, and B. M. Alexandrovich, J. Appl. Phys. **73**, 3657 (1993).
[30]M. Tuszewski and J. A. Tobin, Plasma Sources Sci. Technol. **5**, 640 (1996).
[31]E. L. Tsakadze, K. Ostrikov, Z. L. Tsakadze, S. V. Vladimirov, and S. Xu, Phys. Plasmas **11**, 3915 (2004).
[32]Z. Tsakadze, K. Ostrikov, S. Xu, and E. Tsakadze, Bull. Am. Phys. Soc. **48**(6), 17 (2003).
[33]S. Xu, K. N. Ostrikov, Y. Li, E. L. Tsakadze, and I. R. Jones, Phys. Plasmas **8**, 2549 (2001).
[34]U. Kortshagen, N. D. Gibson, and J. E. Lawler, J. Phys. D **29**, 1224 (1996).
[35]A. I. Smolyakov and I. Khabibrakhmanov, Phys. Rev. Lett. **81**, 4871 (1998).
[36]A. I. Smolyakov, V. Godyak, and A. Duffy, Phys. Plasmas **7**, 4755 (2000).
[37]R. B. Piejak and V. A. Godyak, Appl. Phys. Lett. **76**, 2188 (2000).
[38]Y. Wu and M. A. Lieberman, Plasma Sources Sci. Technol. **9**, 210 (2000).
[39]V. A. Godyak, R. B. Piejak, and B. M. Alexandrovich, Phys. Plasmas **6**, 1804 (1999).